A programmable culture platform for hydrostatic stimulation and in situ pH sensing of lung cancer cells with organic electrochemical transistors

MNE 16 (2022) 100147

Contents lists available at ScienceDirect

Micro and Nano Engineering

journal homepage: www.sciencedirect.com/journal/micro-and-nano-engineering

A programmable culture platform for hydrostatic stimulation and in situ pH sensing of lung cancer cells with organic electrochemical transistors

Cacocciola Nicolò [a,*], Matteo Parmeggiani [a], Simona Villata [a,b], Désirée Baruffaldi [a,b], Simone Luigi Marasso [a,c], Giancarlo Canavese [a], Matteo Cocuzza [a,c], Candido Fabrizio Pirri [a,d], Francesca Frascella [a,b]

[a] DISAT - Politecnico di Torino, Corso Duca degli Abruzzi 24, 10129 Turin, Italy
[b] PolitoBIOMed Lab, Politecnico di Torino, C.so Duca degli Abruzzi 24, 10129 Turin, Italy
[c] CNR-IMEM, Parco Area delle Scienze 37a, 43124 Parma, Italy
[d] Center for Sustainable Future Technologies, Italian Institute of Technology, Via Livorno 60, 10144 Turin, Italy

ARTICLE INFO

Keywords:
Lung-on-a-chip
Bioreactor
Lung cancer
Precision medicine
Organic electrochemical transistors
pH-sensing
PEDOT:PSS

ABSTRACT

In this work, we present a programmable dynamic cell culture stimulation platform designed to work in a CO_2 incubator, compatible with a standard multi-well plate. An epithelial lung cell culture can be mechanically stimulated with a cyclic increase of the hydrostatic pressure inside the culture chamber in the range 1–12 kPa, trying to mimic the human respiration rate. An in situ live pH-monitoring system based on PEDOT:PSS Organic ElectroChemical Transistors was also designed, fabricated and characterized, in order to merge both the stimulated cell culture and the pH sensing in a compact platform.

1. Introduction

Lung cancer is one of the leading causes of death in industrialized countries [1]. Development of cancer therapeutics requires the replacement of costly and time-consuming animal testing with more effective experimental models that go beyond traditional cell cultures in multi-well plates. In the last two decades new fields of research have appeared, moving towards dynamic models in which the organ-specific microenvironment is recreated, in order to maintain cell differentiation and tissue-specific function. Despite the development of a wide variety of sophisticated systems trying to replicate the conditions inside the human organs has been demonstrated, such as the stress conditions which undergoes epithelial tissue in human alveoli and the endothelial tissue surrounding them [2,3], as well as a variety of human organs as kidney [4], liver [5], gut [6] and brain [7], there is a lack of versatile platforms fully compatible with standard cell culture protocols. Moreover, the growth of cultures inside these systems limits the possibility to use multi-well standard detection methods commonly employed in biological laboratories like multi-well plate absorbance reading. An in situ sensing set-up is also needed in order to monitor critical biological, chemical and physical events during the dynamic cell development to better understand the underlying mechanisms of normal lung organogenesis, such as miRNA delivering to neighbouring cells [8] or direct in-vitro monitoring of cell necrosis and early/late apoptosis [9], and also physical quantities such as pH and levels of O_2, NO and glucose [10–13]. The tumor microenvironment is characteristically acidic due to glycolytic cancer cell metabolism, hypoxia and deficient blood perfusion. While in physiological conditions a healthy tissue is around pH 7.4, this value can range from 5.5 to 7.0 in diseased ones [14–17]. Moreover, medium acidosis plays a role in cell cycle, gene expression and cellular metabolism, making in-situ pH sensing a desirable tool to implement during cell culture development [18,19]. Research in the field of pH monitoring in cell cultures has given birth to live-monitoring systems such as microneedles, two-photon fluorescence systems and electronic devices called organic electrochemical transistors (OECTs) [20–22]. They are the most studied novel devices in the field of biosensing, promising advantages such as high sensitivity, high reliability and low cost [23]. In an OECT, the active material forming the transistor channel is made by a conductive polymer, usually the poly(3,4-ethylenedioxythiophene):poly-styrene sulfonate (PEDOT:PSS), a semiconducting material whose channel current (I_{ds}) can be modulated injecting cations coming from the electrolyte solution in which the

* Corresponding author.
E-mail address: nicolo.cacocciola@polito.it (C. Nicolò).

https://doi.org/10.1016/j.mne.2022.100147
Received 20 November 2021; Received in revised form 25 March 2022; Accepted 17 May 2022
Available online 24 May 2022

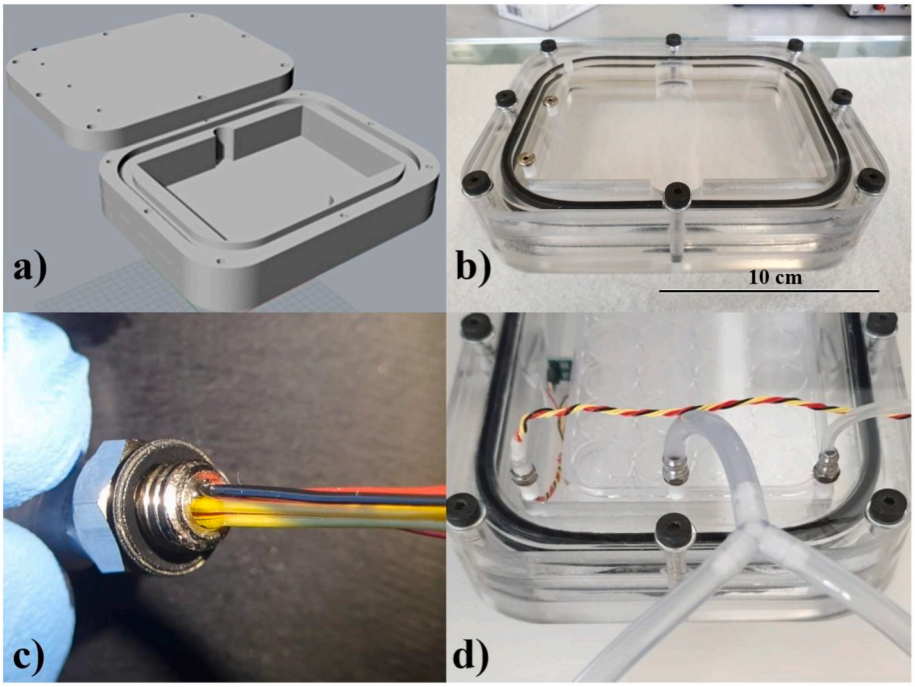

Fig. 1. a) 3D CAD model and b) fabricated PMMA culture chamber. c) Detail of the temperature sensor's feed-through sealed with PDMS. d) Detail of the lid: from left to right, temperature sensor, pump/solenoid valve inlet, pressure sensor sampling port.

device is immersed, by applying a positive gate voltage (V_G), being able to easily work in the cell culture medium [24]. This class of devices has been widely studied for applications in biological environments, for applications such as biosensing of target analytes upon proper functionalization of the gate electrode, membrane permeability studies on cell layers, cell migration, ion signalling and measuring neural activity in vivo [25–27]. The work proposed in this paper aims to build a platform designed for the growth of both healthy and tumor lung cells compatible with standard multi-well plate culture protocols, in which cells are subjected to a mechanical stimulus given by the cyclic increase of the hydrostatic pressure inside the culture chamber mimicking a physiological breathing cycle. On the other hand, an increase in hydrostatic pressure leads to an increase of the partial pressure of gases in the culture chamber, in particular of CO_2, which once dissolved in water can lead to the formation of carbonic acid, therefore lowering the pH value of culture media [28,29]. The system is thus also equipped with an array of PEDOT:PSS based OECTs designed to work directly inside the system, in order to monitor pH changes in culture media during cell development, and to investigate the dynamics of this parameter when both healthy and tumor cell cultures are stressed with an hydrostatic stimulus.

2. Materials and methods

2.1. PMMA culture chamber fabrication

The cell culture chamber was designed with a 3D CAD tool (Rhinoceros®, Robert McNeel & Associates) and then manufactured using a numerically controlled milling machine (Benchman VMC 4000).

The chamber consists of 3 panels of Polymethylmethacrylate (PMMA) hollowed to contain a multi-well plate of standard dimensions, and then assembled in a sandwich structure and fixed with 8 steel screws. The tightness of the chamber is ensured by a pair of nitrile rubber O-rings, arranged in a groove between each pair of panels, after greasing them with vacuum grease. The top panel is designed with 3 feed-through holes to which it is possible to connect the chamber pressurization system, the temperature sensor, and the differential pressure sensor. The feed-through for the temperature sensor was fabricated by means of a pneumatic connection, which was suitably sealed with PDMS (Sylgard® 184, 1:10 ratio) to maintain the airtight seal of the chamber (Fig. 1).

2.2. Electronic control system

The electronic control system consists of six different main blocks (Fig. 2c). A microcontroller unit (MCU), implemented using an Arduino Nano® microcontroller, provides the features to program the platform and regulate the on/off cycles of a diaphragm air pump and the solenoid valve and its duration to reach the desired pressure inside the chamber, and also to manage data coming from the temperature sensor and the differential pressure sensor connected to the culture chamber. The differential pressure sensor (NPX MPX5100DP) is connected to the Arduino board which provides power supply and manage the sensor's analogue output, while the temperature sensor's output (Honeywell HIH6130 series) makes use of the I^2C protocol to communicate with the Arduino board, from which it is also powered. The remaining three main blocks are quite similar, consisting in three different dedicated power supply lines based on the LM317/NOPB linear voltage regulator (Texas Instruments), one line providing a fixed DC output of 9 V to the Arduino board, and two DC outputs to the diaphragm pump and the solenoid valve, adjustable between 3 and 12 V in order to variate the input and output air flux in the chamber, and consequently the maximum pressure reached in each cycle by the system.

2.3. OECTs design and fabrication

The OECTs were fabricated in a clean room environment on a 4" SiO_2 finished p-type (100) silicon wafer. In view of their future application, which will consist in the use of devices while immersed in the low cell culture medium volumes of a multi-well plate, the source and drain electrodes have been designed with an interdigitated geometry, which allows to have chips of considerably reduced dimensions, and to remarkably increase the W/L ratio of the devices, which in this case were designed to be of W = 9.99 mm and L = 10 μm. The Au source and

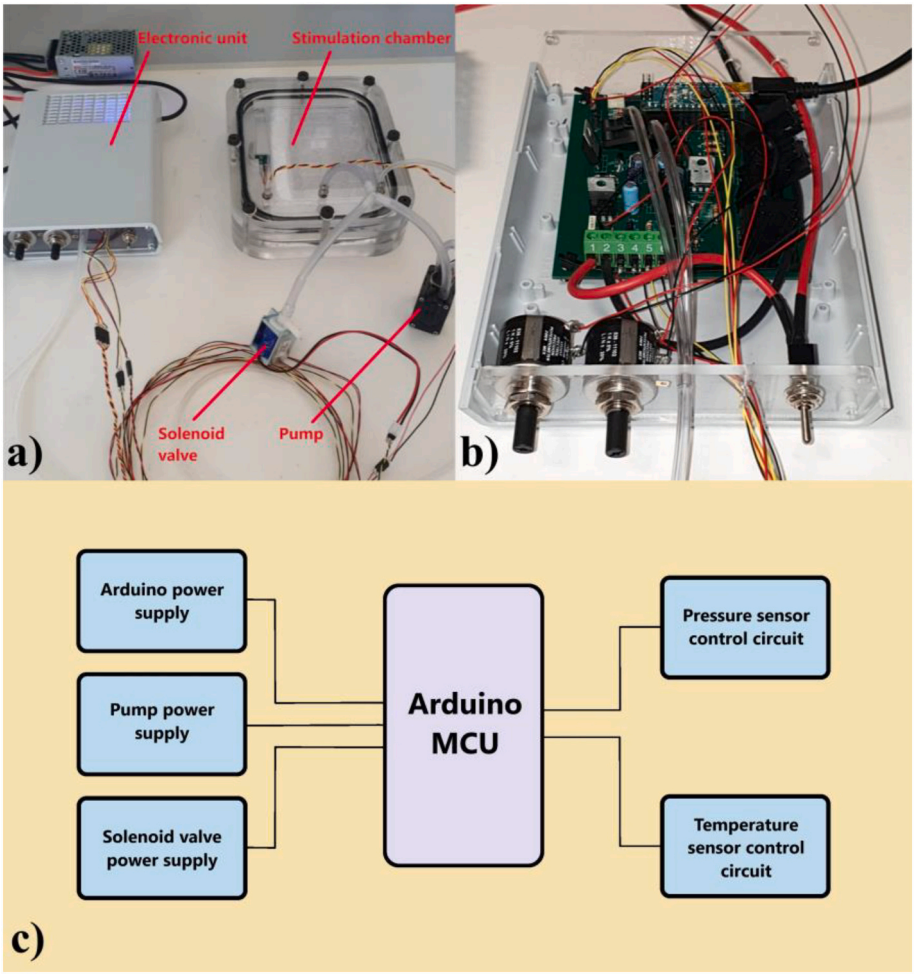

Fig. 2. a) overview of the entire system. b) Detail of the electronic control circuit assembled inside its case. c) Electronic diagram of the control circuit and its main blocks.

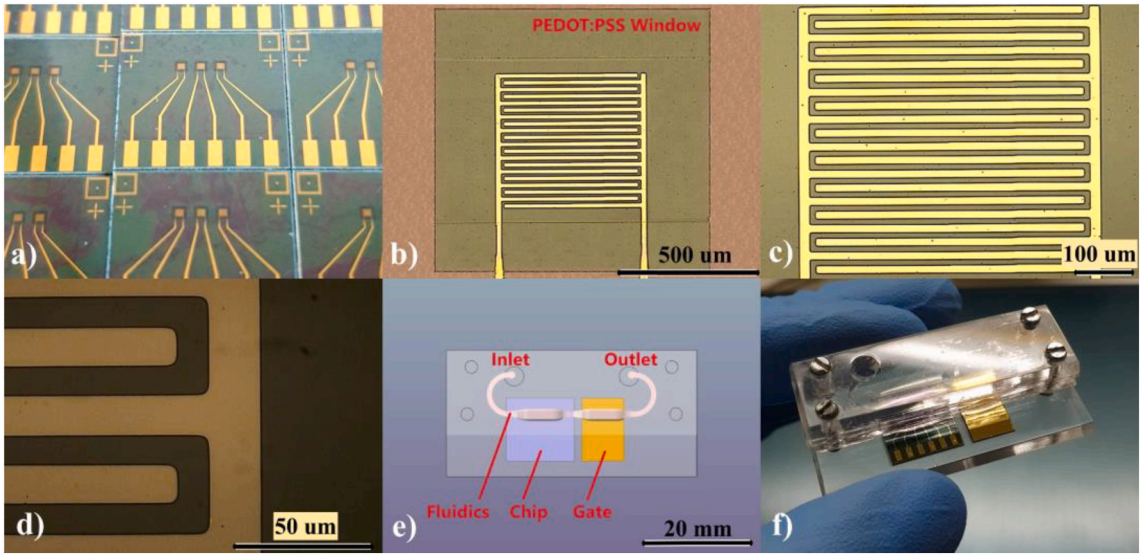

Fig. 3. a) view of the fabricated OECTs on a silicon wafer. b), c), d) Close view of the interdigitated source and drain electrodes and PEDOT:PSS window. e) CAD view of the assembled device with fluidics and gate electrode. f) Picture of the device assembled.

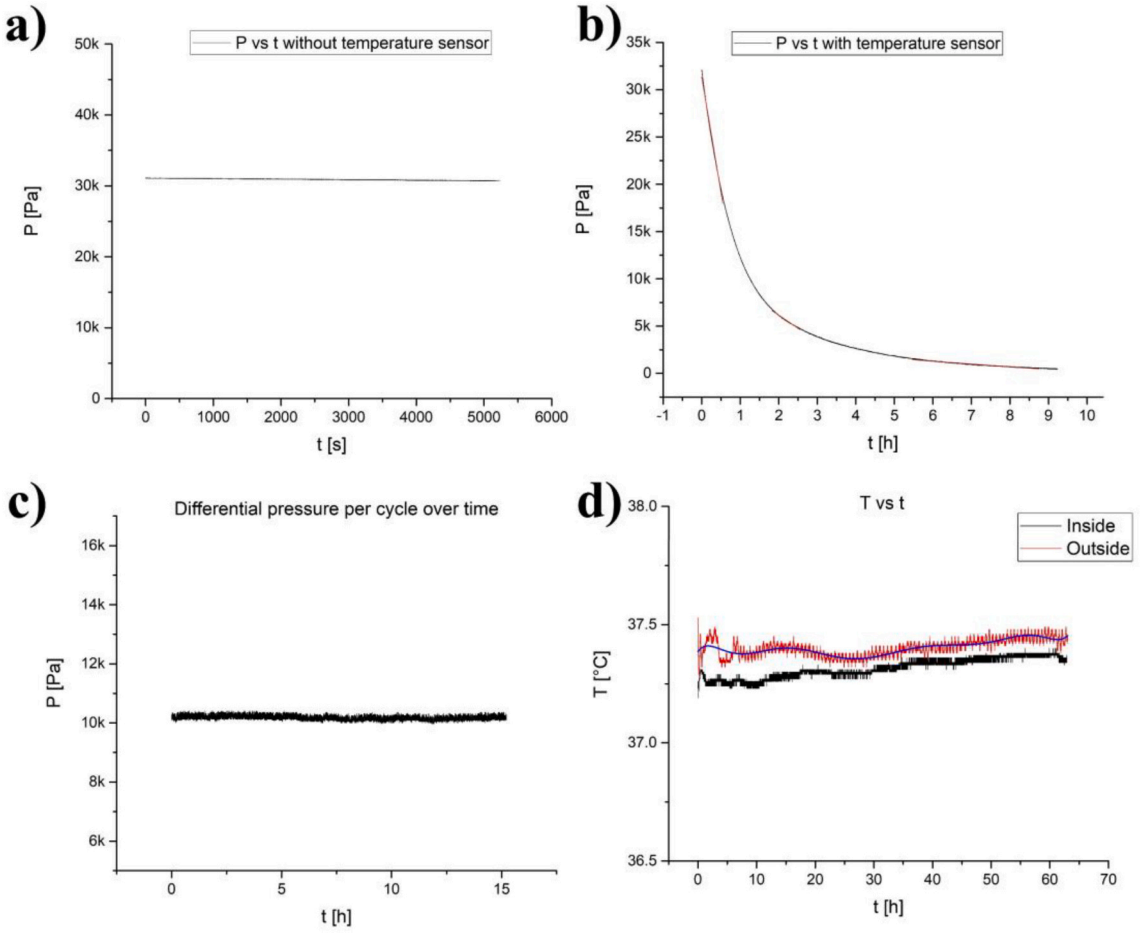

Fig. 4. Pressure vs time inside the chamber without (a) and with (b) temperature sensor. c) Differential pressure reached at each cycle over time. d) Temperature monitoring inside and outside the chamber, performed in a CO_2 incubator.

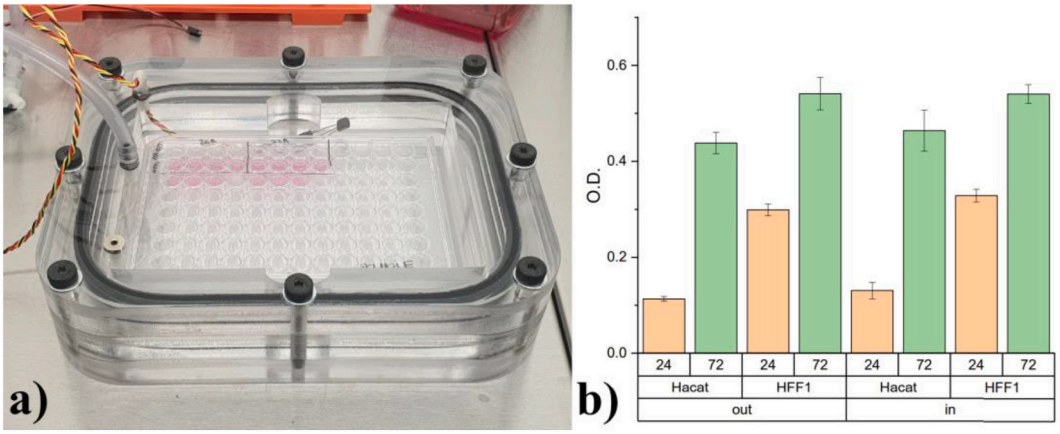

Fig. 5. a) HaCaT and HFF-1 experimental setup in a 96-well plate placed in the culture chamber. b) Optical density (570/650 nm) was read at 24 h and 72 h. Standard culture conditions (out) were used as control. The results were shown as mean ± standard deviation.

drain electrodes of the devices were fabricated by e-beam evaporation and lift-off processes. An Al_2O_3 passivation layer has been deposited with the same technique on the chips, leaving one window on the pads and one on the interdigitated source and drain electrodes, following a well established procedure [30]. On the latter, a 200 nm thick layer of PEDOT:PSS was then deposited by spin coating and patterned by photolithography and reactive ion etching. The detailed fabrication procedure is reported in supporting information. The chip and the gate electrode are finally assembled in a fluidic system, in which the devices are exposed to the electrolyte solution by inserting it in the inlet (Fig. 3e). Electrical characterizations are performed by contacting the electrical pads from the outside of the system, as shown in Fig. 3 f.

2.4. Cell viability assay

For cell survival assessment, two normal cell lines were selected:

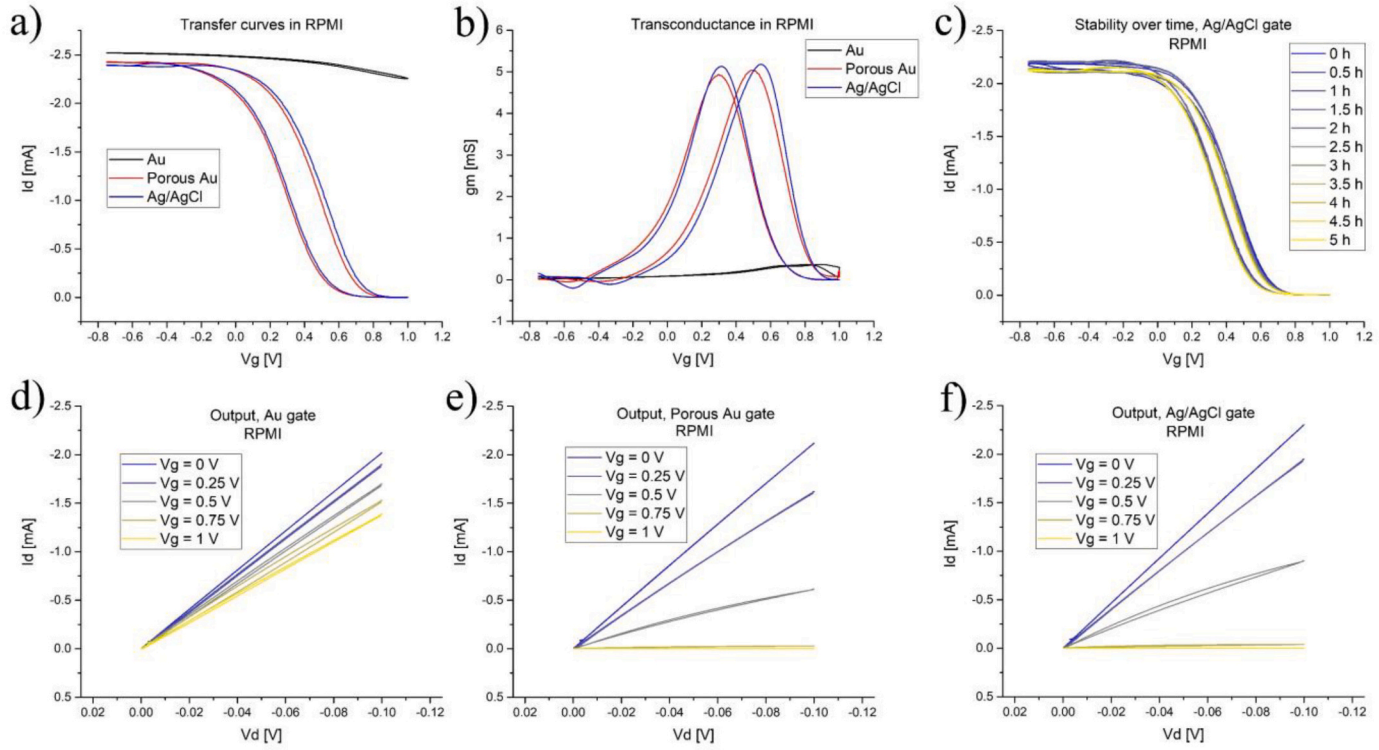

Fig. 6. a) Trans-characteristic (transfer) curves of the devices tested in cell culture media with three different gate electrodes: Au, porous Au, and Ag/AgCl. b) Transconductance of the devices. c) Stability test performed on the devices in cell culture media. d), e), f) Output curves of the devices tested in cell culture media, from left to right: Au gate, porous Au, Ag/AgCl.

Table 1
Main key parameters extracted from the electrical characterization of the devices. In the case of evaporated Au, I_{ON}/I_{OFF} is not shown, as the device does not turn off with this gate electrode.

Gate electrode	gm_{MAX}	$V_{G\|gmMAX}$	I_{ON}/I_{OFF}	ΔV_G hysteresis @gm_{MAX}
Evaporated Au	0.4 mS	0.9 V	–	41 μV
Porous Au	5.0 mS	0.49 V	3001	195 mV
Ag/AgCl	5.2 mS	0.51 V	2738	230 mV

Human epidermal keratinocyte line (HaCaT) and Human foreskin fibroblasts line (HFF-1). Cells were cultured in DMEM GLUTAMAX (Gibco, ThermoFisher Scientific) with the addition of 15% Fetal Bovine Serum (Sigma-Aldrich), 1% L-Glutammine (Sigma-Aldrich), 1% Penicillin Streptomycin (Sigma-Aldrich) and 1% Sodium Pyruvate (Sigma-Aldrich). HFF1 and HaCaT were plated at the density of 10^4 cells/well and 7000 cells/well respectively in a 96-well plate. Metabolic activity was analysed 24 h and 72 h after seeding by MTT assay (Thiazolyl blue formazan, Sigma-Aldrich). Cells were incubated with 0.5 mg/ml MTT at 37 °C for 2 h and then, formed salts were dissolved in MTT solvent (10% SDS, 0.01 M HCl in H2O) at 37 °C for 1 h. The absorbance was read at 570 nm (650 nm reference wavelength) using a Synergy™ HTX Multi-Mode Microplate Reader (BioTek, Winoosky, Vermont, USA).

3. Results

3.1. Culture chamber characterization

The culture chamber system and its electronics were characterized in order to test the airtightness of the chamber, the repeatability of the pressure cycles over time, and to monitor any temperature variation induced by the pressurization/depressurization cycles compared to the chamber outside. Since the PDMS feed-through of the temperature sensor represents a major leakage source for the chamber, two different preliminary sealing tests were made, without and with the feed-through (replacing it with a sealing cap), to evaluate the order of magnitude of the phenomenon. In the first case, the leakage showed a constant trend as shown in Fig. 4a, which turned out to be equal to −0.16 Pa/s. In the second case, the leakage showed a negative exponential trend, (Fig. 4b). A linear fit was calculated in three different intervals where the curve shows a significantly different trend, resulting in three different pressure decrease trends which turned out to be equal to −6.78, −0.77 and −0.08 Pa/s. Considering the final pressure range reached by the system in steady-state (0.5–12 kPa, period 5 s), in both cases it resulted in a leakage negligible for the application. The repeatability of the pressure cycles was also tested, setting a differential overpressure of 11 kPa.

The data acquired by the pressure sensor highlighted a maximum pressure shift of 0.153 Pa, as shown in Fig. 4c, which is less than the maximum error reported on the sensor's datasheet, which is 2.5% between 0° and 85 °C. The temperature inside and outside the chamber was also monitored over time in a CO_2 incubator (ThermoFisher Scientific Heracell® 150i), with standard environmental values for cell culture growth (37 °C, 95% RH, 5% CO_2). The results highlighted in Fig. 4d, show the temperature trend inside and outside the culture chamber, indicating a mean temperature of 37,31 °C inside and 37,40 °C outside. The maximum temperature shift observed turned out to be 0.23 °C, which is less than the maximum temperature error reported in the sensor's datasheet, which is 0.5 °C in the range 5° - 50 °C.

3.2. HaCaT and HFF-1 proliferation test

Preliminary proliferation tests were performed inside the culture chamber, setting the pressure cycles at 12 kPa, with a period of 5 s. Cells grown in standard conditions were used as control. Human epidermal keratinocyte line (HaCaT) and Human foreskin fibroblasts line (HFF-1) cultures were grown in replicates ($n = 3$) with an extra-filled well working as reference, as shown in Fig. 5 and cell proliferation was

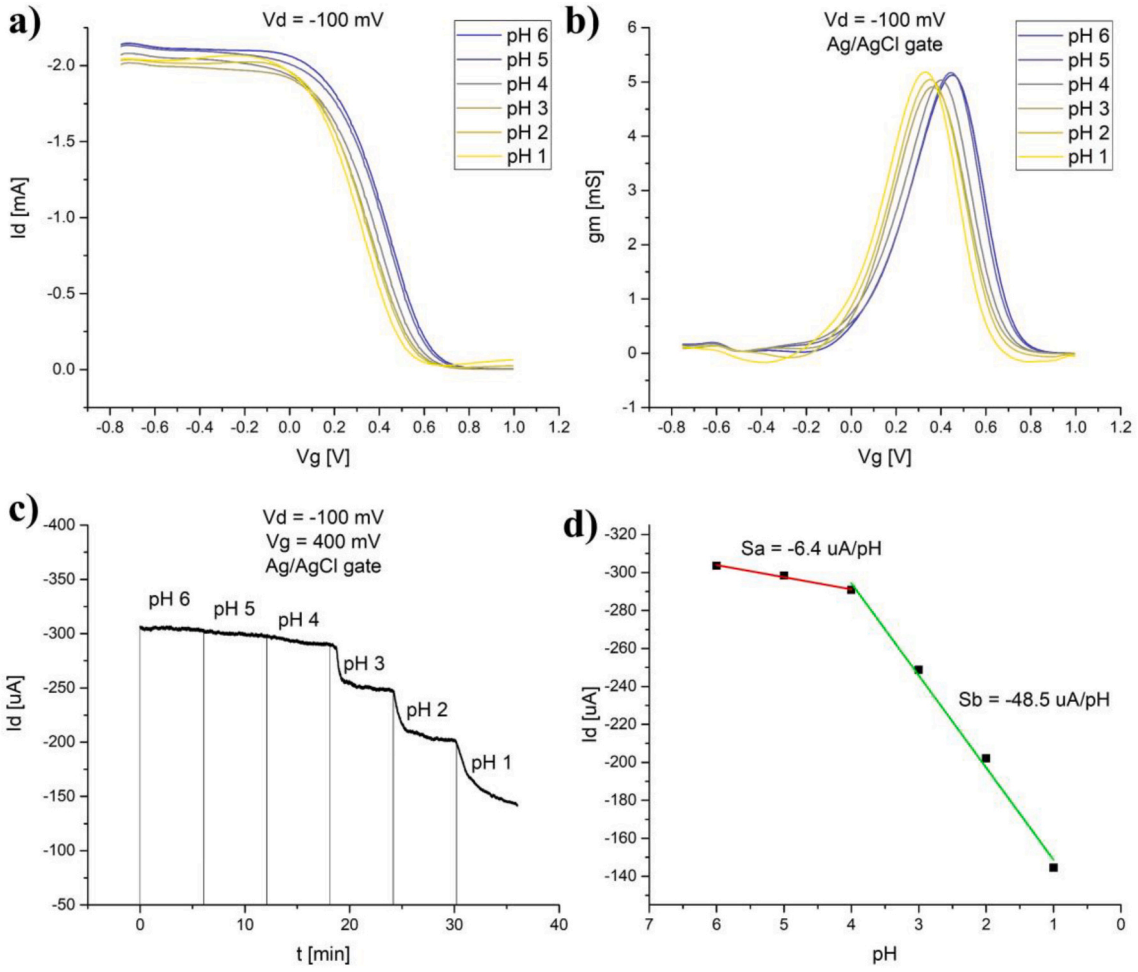

Fig. 7. (a) Transfer curves and (b) transconductance curves of the devices tested in a solution of NaCl 0.1 M with different concentrations of HCl (0.1 M – 10^{-6} M), with a resulting pH ranging from 1 to 6 respectively. c) real time test showing the response of the device to the flux of the electrolyte solution with increasing acidity d) plot of the drain current as a function of the pH. The slope of the linear least square fit gives the resulting sensitivities Sa and Sb.

Table 2
main key parameters extracted from the electrical characterization of the devices using solutions of NaCl 0.1 M with different concentrations of HCl (0.1 M – 10^{-6} M), with a resulting pH ranging from 1 to 6 respectively. Last column shows the voltage shift compared to pH 6.

pH	gm_{MAX}	$V_{G\|gmMAX}$	I_{ON}/I_{OFF}	ΔV_G shift pH 6 @gm_{MAX}
6	5.1 mS	0.45 V	474	–
5	5.2 mS	0.44 V	854	10 mV
4	5.0 mS	0.40 V	773	50 mV
3	4.9 mS	0.36 V	669	90 mV
2	5.0 mS	0.35 V	135	100 mV
1	5.2 mS	0.33 V	103	120 mV

monitored reading the optical density in both plates after 24 h and 72 h. As shown in Fig. 5b, signal increase was observed at 72 h compared to the 24 h one for all the culture conditions. Interestingly, no differences were detected when cells were subjected to pressure cycles, suggesting the absence of effects on cell proliferation. In future, further analysis will be performed with other cell types and pressure values, to see if such changes in culture conditions will induce differences in cell response in terms of cell proliferation, viability and gene activation.

3.3. OECT electrical characterization

The OECTs were characterized connecting the source, the drain and the gate electrodes to a programmable source meter (Keysight Technologies B2912A). Both the gate and the drain voltages were referred to the source voltage, which was connected to ground. Tests with different gate materials have been carried out on the devices using cell culture media as an electrolyte solution. Three different gate electrodes were used, namely an electron-beam evaporated Au electrode, a porous Au gate electrode, and a Ag/AgCl wire electrode. The gate area exposed to the electrolyte solution was equal to 9 mm^2 in each case. The transfer curves have been obtained modulating the gate voltage between −0.75 and 1 V with a scan rate of 125 mV/s, while the drain voltage was set to −100 mV. The results, highlighted in Fig. 6, show different behaviours between the different gate materials. Both the porous Au gate and the Ag/AgCl gate effectively decrease the drain current of the device as the gate voltage increases, turning it off for $V_G > 0.8$ V. Using the evaporated Au gate, this does not happen, probably because in this case the capacitance associated with the channel-electrolyte (C_{CH}) interface is much greater than the one associated with the gate-electrolyte interface (C_G). This phenomenon is confirmed by the fact that porous Au, with the same exposed gate area, offers an effective area 20 times greater than that of evaporated Au, which results in a greater C_G. The gate voltage corresponding to the maximum transconductance value on the devices turned out to be 0.9 V for the evaporated Au electrode, 0.49 V for the porous Au gate and 0.51 V for the Ag/AgCl gate, with a maximum transconductance of 0.4, 5.0 and 5.2 mS respectively. Stability tests were also performed on the devices with an Ag/AgCl gate electrode, due to its higher transconductance and reliability compared to the other two

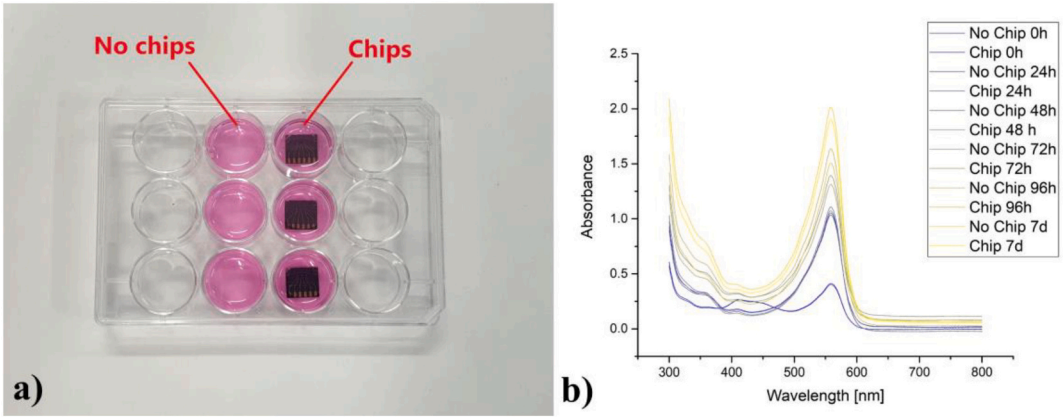

Fig. 8. a) Experimental setup for the colour monitoring of cell culture media. b) Resulting absorbance spectrum checked every 24 h.

gate materials. For this test the cell culture media was again used as an electrolyte solution, to further verify the operation of the devices within the cell growth environment. The gate voltage has been set between −0.75 and 1 V with a scan rate of 125 mV/s, while the drain voltage was set to −100 mV. In the test, highlighted in Fig. 6 c), the single transfer curves have been obtained inserting a 30 min rest pause between them. The devices showed an absolute current shift over time equal to 158 μA at the maximum transconductance point of the curve (V_G = 0.51 V), which represents a relative current shift equal to 7.3%. The main figures of merit of the single devices for the three gate electrodes are summarized in Table 1.

3.4. pH-related electrical response of OECT

The electrical response of the devices in electrolyte solutions with different pH values has been investigated using six different solutions, with an increasing concentration of HCl ranging from 0.1 M (pH 1) to 10^{-6} M (pH 6), and a fixed concentration of NaCl (0.1 M). All the tests have been performed with an Ag/AgCl gate electrode, with V_G ranging from −0.75 to 1 V, V_D = −100 mV and a scan rate of 125 mV/s. The results, shown in Fig. 7a and 7b, exhibit a well-marked shift of the transfer curves (and thus of the gm_{MAX}) at lower V_G values as the pH of the solution decreases. The main figures of merit of the devices in such conditions are summarized in Table 2. The response of the device to different pH can be monitored by measuring the shift of the transfer curves, which is well described by the position of the transconductance peak ($V_G|_{gmMAX}$). As can be noted from Table 2, the peak position shifts towards lower gate voltages when the pH is reduced. This behaviour was expected, since as the pH value decreases, the concentration of dissociated H^+ ions inside it increases by an order of magnitude for each pH unit. Consequently, for a fixed V_G more of these positive ions are injected in the polymer film from the electrolyte, which translates into a greater ability to shut off the drain current. A real-time test was also carried out, fixing V_G = 400 mV, V_D = −100 mV, and fluxing each solution for 360 s inside the fluidics with a flow rate of 100 μl/min, starting from the less acidic one (pH 6) to the most acidic one (pH 1). The results, as we can see in Fig. 7c, show a slight decrease of the absolute value of the drain current in the case of the first three solutions (group 1, pH = 6, 5, 4) and a well-marked decrease of the drain current for the remaining three solutions (group 2, pH = 3, 2, 1). Fig. 7d shows the sensitivity of the device for these two groups of pH values, resulting in Sa = −6.4 μA/pH for the first group and Sb = −48.5 μA/pH for the second group.

3.5. Preliminary absorbance perturbation test with OECTs in culture media

In order to show the non-alteration of the pH of the cell culture media by the presence of the OECTs, an absorbance perturbation test was carried out as follows. Given the nature of the cell culture media, which contains phenol red as an indicator of pH, changing from yellow to bright pink in the pH range between 6.8 and 8.2, a variation in the absorbance spectrum in the cell culture media reflects a variation in its pH. Given the pH-monitoring application for which the OECTs of this work are intended, a preliminary absorbance perturbation test was performed in cell culture media (RPMI 1640, GlutaMAX™, Gibco ThermoFisher Scientific), dipping the chips (not biased) inside it in replicates (n = 3) and monitoring the absorbance of the culture media in the spectrum between 300 and 800 nm every 24 h (Fig. 8a). Such absorbance was compared to a replicate of the same culture media (n = 3) working as reference, subtracting from their spectra the one coming from the multi-well plate material itself, working as blank. As shown in Fig. 8b, no absorbance variation has been observed during 7 days among the wells, showing a stable absorbance peak at a wavelength of 559 nm. This can be translated in an apparent non-variation of the pH in the culture medium, or of a variation thereof which cannot be detected by this measurement system.

4. Conclusions and future outlooks

This work shows the feasibility of using our device as cell culture chamber, in which it is possible to apply a cyclic increase of the hydrostatic pressure without causing damage to the cells. It is worth mentioning that, given the absence of effects on the cell proliferation during operation inside the system, the cyclic increase of the hydrostatic pressure does not affect this parameter, but could influence cytoskeletal stiffness/rearrangements, which will be monitored in the future tests. Moreover, cell migration and wound healing will be analysed to assess the effects of cytoskeletal changing on these features. OECTs have been also demonstrated to work in a stable manner inside the culture media, without changing its pH, after being immersed inside it over a week. Future tests will be performed inside the chamber using different values of hydrostatic pressure, involving this time human alveolar epithelial cells and human adenocarcinomic alveolar epithelial cells (A549 cell line), studying key parameters related to their growth. Further tests on the pH response of the OECTs will also be performed, in view of their use to real time monitor parameters during the cell growth. Both the culture chamber and the OECTs are also enough versatile to explore, in the near future, different live monitoring paths, not only pH but also the detection of specific fingerprint analytes related with tumor cells development, upon proper functionalization of the gate electrode.

Declaration of Competing Interest

The Authors declare no conflict of interest. The authors declares that they have no relevant or material financial interests that relate to the research described in this work. The present work was performed in the

framework of DEFLeCT (“Advanced platform for the early detection of not small cells lung cancer”) project, financed by Piedmont Region in the framework of “Health & WellBeing” Platform project.

References

[1] Cancer. https://www.who.int/news-room/fact-sheets/detail/cancer.

[2] B.A. Hassell, G. Goyal, E. Lee, A. Sontheimer-Phelps, O. Levy, C.S. Chen, D. E. Ingber, Human organ chip models recapitulate orthotopic lung cancer growth, therapeutic responses, and tumor dormancy in vitro, Cell Rep. 21 (2) (2017) 508–516, https://doi.org/10.1016/j.celrep.2017.09.043.

[3] J. Shrestha, S. Razavi Bazaz, H. Aboulkheyr Es, D. Yaghobian Azari, B. Thierry, M. Ebrahimi Warkiani, M. Ghadiri, Lung-on-a-chip: the future of respiratory disease models and pharmacological studies, Crit. Rev. Biotechnol. 40 (2) (2020) 213–230, https://doi.org/10.1080/07388551.2019.1710458.

[4] J. Wang, C. Wang, N. Xu, Z.-F. Liu, D.-W. Pang, Z.-L. Zhang, A virus-induced kidney disease model based on organ-on-a-chip: pathogenesis exploration of virus-related renal dysfunctions, Biomaterials 219 (2019), 119367, https://doi.org/10.1016/j.biomaterials.2019.119367.

[5] N.S. Bhise, V. Manoharan, S. Massa, A. Tamayol, M. Ghaderi, M. Miscuglio, Q. Lang, Y. Shrike Zhang, S.R. Shin, G. Calzone, N. Annabi, T.D. Shupe, C. E. Bishop, A. Atala, M.R. Dokmeci, A. Khademhosseini, A liver-on-a-chip platform with bioprinted hepatic spheroids, Biofabrication 8 (1) (2016), 014101, https://doi.org/10.1088/1758-5090/8/1/014101.

[6] P. de Haan, M.A. Ianovska, K. Mathwig, G.A.A. van Lieshout, V. Triantis, H. Bouwmeester, E. Verpoorte, Digestion-on-a-chip: a continuous-flow modular microsystem recreating enzymatic digestion in the gastrointestinal tract, Lab Chip 19 (9) (2019) 1599–1609, https://doi.org/10.1039/C8LC01080C.

[7] J. Park, B.K. Lee, G.S. Jeong, J.K. Hyun, C.J. Lee, S.-H. Lee, Three-dimensional brain-on-a-chip with an interstitial level of flow and its application as an in vitro model of Alzheimer’s disease, Lab Chip 15 (1) (2015) 141–150, https://doi.org/10.1039/C4LC00962B.

[8] T. Najrana, A. Mahadeo, R. Abu-Eid, E. Kreienberg, V. Schulte, A. Uzun, C. Schorl, L. Goldberg, P. Quesenberry, J. Sanchez-Esteban, Mechanical stretch regulates the expression of specific MiRNA in extracellular vesicles released from lung epithelial cells, J. Cell. Physiol. 235 (11) (2020) 8210–8223, https://doi.org/10.1002/jcp.29476.

[9] A. Romeo, G. Tarabella, P. D’Angelo, C. Caffarra, D. Cretella, R. Alfieri, P. G. Petronini, S. Iannotta, Drug-induced cellular death dynamics monitored by a highly sensitive organic electrochemical system, Biosens. Bioelectron. 68 (2015) 791–797, https://doi.org/10.1016/j.bios.2015.01.073.

[10] J.J. Davenport, M. Hickey, J.P. Phillips, P.A. Kyriacou, Dual PO $_2$/PCO $_2$ fibre optic sensing film, Analyst 142 (10) (2017) 1711–1719, https://doi.org/10.1039/C7AN00173H.

[11] L. Ding, C. Fan, Y. Zhong, T. Li, J. Huang, A sensitive optic fiber sensor based on CdSe QDs fluorophore for nitric oxide detection, Sensors Actuators B Chem. 185 (2013) 70–76, https://doi.org/10.1016/j.snb.2013.04.092.

[12] A. Deep, U. Tiwari, P. Kumar, V. Mishra, S.C. Jain, N. Singh, P. Kapur, L. M. Bharadwaj, Immobilization of enzyme on long period grating fibers for sensitive glucose detection, Biosens. Bioelectron. 33 (1) (2012) 190–195, https://doi.org/10.1016/j.bios.2011.12.051.

[13] D. Choudhury, M.G. Tanner, S. McAughtrie, F. Yu, B. Mills, T.R. Choudhary, S. Seth, T.H. Craven, J.M. Stone, I.K. Mati, C.J. Campbell, M. Bradley, C.K. I. Williams, K. Dhaliwal, T.A. Birks, R.R. Thomson, Endoscopic sensing of alveolar PH, Biomed. Opt. Express 8 (1) (2017) 243, https://doi.org/10.1364/BOE.8.000243.

[14] C. Justus, E. Sanderlin, L. Yang, Molecular connections between cancer cell metabolism and the tumor microenvironment, Int. J. Mol. Sci. 16 (12) (2015) 11055–11086, https://doi.org/10.3390/ijms160511055.

[15] S. Romero-Garcia, H. Prado-Garcia, A.D. Valencia-Camargo, A. Alvarez-Pulido, Lactic acidosis promotes mitochondrial biogenesis in lung adenocarcinoma cells, supporting proliferation under Normoxia or survival under hypoxia, Front. Oncol. 9 (2019) 1053, https://doi.org/10.3389/fonc.2019.01053.

[16] P. Vaupel, H. Schmidberger, A. Mayer, The Warburg effect: essential part of metabolic reprogramming and central contributor to cancer progression, Int. J. Radiat. Biol. 95 (7) (2019) 912–919, https://doi.org/10.1080/09553002.2019.1589653.

[17] V. L, D. R, L. Dong, Targeting tumor microenvironments for cancer prevention and therapy, in: A.G. Georgakilas (Ed.), Cancer Prevention - From Mechanisms to Translational Benefits, InTech, 2012, https://doi.org/10.5772/28692.

[18] W. Liu, Z. Ren, K. Lu, C. Song, E.C.W. Cheung, Z. Zhou, G. Chen, The suppression of medium acidosis improves the maintenance and differentiation of human pluripotent stem cells at high density in defined cell culture medium, Int. J. Biol. Sci. 14 (5) (2018) 485–496, https://doi.org/10.7150/ijbs.24681.

[19] Y. Wu, B. Gao, Q.-J. Xiong, Y.-C. Wang, D.-K. Huang, W.-N. Wu, Acid-sensing ion channels contribute to the effect of extracellular acidosis on proliferation and migration of A549 cells, Tumor Biol. 39 (6) (2017), https://doi.org/10.1177/1010428317705750, 101042831770575.

[20] I.L. Moldero, A. Chandra, M. Cavo, C. Mota, D. Kapsokalyvas, G. Gigli, L. Moroni, L. L. Mercato, Probing the PH microenvironment of mesenchymal stromal cell cultures on additive-manufactured scaffolds, Small 16 (34) (2020) 2002258, https://doi.org/10.1002/smll.202002258.

[21] J. Ge, L. Fan, K. Zhang, T. Ou, Y. Li, C. Zhang, C. Dong, S. Shuang, M.S. Wong, A two-photon ratiometric fluorescent probe for effective monitoring of lysosomal PH in live cells and cancer tissues, Sensors Actuators B Chem. 262 (2018) 913–921, https://doi.org/10.1016/j.snb.2018.02.082.

[22] G. Scheiblin, R. Coppard, R.M. Owens, P. Mailley, G.G. Malliaras, Referenceless PH sensor using organic electrochemical transistors, Adv. Mater. Technol. 2 (2) (2017) 1600141, https://doi.org/10.1002/admt.201600141.

[23] E. Macchia, P. Romele, K. Manoli, M. Ghittorelli, M. Magliulo, Z.M. Kovács-Vajna, F. Torricelli, L. Torsi, Ultra-sensitive protein detection with organic electrochemical transistors printed on plastic substrates, Flex. Print. Electron. 3 (3) (2018), 034002, https://doi.org/10.1088/2058-8585/aad0cb.

[24] K. Lieberth, P. Romele, F. Torricelli, D.A. Koutsouras, M. Brückner, V. Mailänder, P. Gkoupidenis, P.W.M. Blom, Current-driven organic electrochemical transistors for monitoring cell layer integrity with enhanced sensitivity, Adv. Healthc. Mater. 10 (19) (2021) 2100845, https://doi.org/10.1002/adhm.202100845.

[25] L. Chen, Y. Fu, N. Wang, A. Yang, Y. Li, J. Wu, H. Ju, F. Yan, Organic electrochemical transistors for the detection of cell surface Glycans, ACS Appl. Mater. Interfaces 10 (22) (2018) 18470–18477, https://doi.org/10.1021/acsami.8b01987.

[26] D. Khodagholy, T. Doublet, P. Quilichini, M. Gurfinkel, P. Leleux, A. Ghestem, E. Ismailova, T. Hervé, S. Sanaur, C. Bernard, G.G. Malliaras, In vivo recordings of brain activity using organic transistors, Nat. Commun. 4 (1) (2013) 1575, https://doi.org/10.1038/ncomms2573.

[27] Y. Lee, G. Lee, M. Cho, J.-K. Park, Design criteria and standardization of a microfluidic cell culture system for investigating cellular migration, J. Micromech. Microeng. 29 (4) (2019), 043003, https://doi.org/10.1088/1361-6439/ab0796.

[28] C. Peng, J.P. Crawshaw, G.C. Maitland, J.P. Martin Trusler, D. Vega-Maza, The PH of CO2-saturated water at temperatures between 308K and 423K at pressures up to 15MPa, J. Supercrit. Fluids 82 (2013) 129–137, https://doi.org/10.1016/j.supflu.2013.07.001.

[29] B. Meyssami, M.O. Balaban, A.A. Teixeira, Prediction of PH in model systems pressurized with carbon dioxide, Biotechnol. Prog. 8 (2) (1992) 149–154, https://doi.org/10.1021/bp00014a009.

[30] M. Segantini, M. Parmeggiani, A. Ballesio, G. Palmara, F. Frascella, S.L. Marasso, M. Cocuzza, Design of a portable microfluidic platform for EGOT-based in liquid biosensing, Sensors 22 (3) (2022) 969, https://doi.org/10.3390/s22030969.